Gravitational Radiation from Rotational Core Collapse: Effects of Magnetic Fields and Realistic Equation of States

Kei Kotake,[1,*] Shoichi Yamada,[2] Katsuhiko Sato,[1,3]
Kohsuke Sumiyoshi,[4] Hiroyuki Ono,[5] and Hideyuki Suzuki[5]

[1]*Department of Physics, School of Science, the University of Tokyo, 7-3-1 Hongo, Bunkyo-ku, Tokyo 113-0033, Japan*

[2]*Science & Engineering, Waseda University, 3-4-1 Okubo, Shinjuku, Tokyo, 169-8555, Japan*

[3]*Research Center for the Early Universe, School of Science, the University of Tokyo, 7-3-1 Hongo, Bunkyo-ku, Tokyo 113-0033, Japan*

[4]*Numazu College of Technology, Ooka 3600, Numazu, Shizuoka 410-8501, Japan*

[5]*Faculty of Science and Technology, Tokyo University of Science, Yamazaki 2641, Noda, Chiba, 278-8510, Japan*

(Dated: February 2, 2008)

Abstract

We perform a series of two-dimensional, axisymmetric, magnetohydrodynamic simulations of the rotational collapse of a supernova core. In order to calculate the waveforms of the gravitational wave, we derive the quadrupole formula including the contributions from the electromagnetic fields. Recent stellar evolution calculations imply that the magnetic fields of the toroidal components are much stronger than those of the poloidal ones at the presupernova stage. Thus, we systematically investigate the effects of the toroidal magnetic fields on the amplitudes and waveforms of the gravitational wave. Furthermore, we employ the two kinds of the realistic equation of states, which are often used in the supernova simulations. Then, we investigate the effects of the equation of states on the gravitational wave signals. As for the microphysics, we took into account electron capture and neutrino transport by the so-called leakage scheme. With these computations, we find that the peak amplitudes of the gravitational wave are lowered by an order of 10% for the models with the strongest toroidal magnetic fields. However, the peak amplitudes are mostly within the sensitivity range of laser interferometers such as TAMA and the first LIGO for a source at a distance of 10 kpc. Furthermore, we point out that the amplitudes of second peaks are still within the detection limit of the first LIGO for the source, although the characteristics of second peaks are reduced by the magnetic fields. We stress the importance of the detection, since it will give us information about the angular momentum distribution of massive evolved stars. When we compare the gravitational waves from the two realistic equation of states, significant differences are not found, except that the typical frequencies of the gravitational wave become slightly higher for the softer equation of state.

PACS numbers: 04.30.Db

*E-mail: kkotake@utap.phys.s.u-tokyo.ac.jp

I. INTRODUCTION

Rotation has been supposed to play an important role in the gravitational radiation from core collapse supernovae. The large-scale asphericities at core bounce induced by rotation can convert the part of the gravitational energy into the form of the gravitational waves. The expected amplitude of the gravitational waves from a supernova in the Milky Way is considered to be within the detection limits of the long-base line laser interferometers such as [GEO600, LIGO, TAMA, VIRGO] [1]. The detection of the gravitational wave is important not only for itself but also for the understanding of core collapse supernovae themselves, because the gravitational wave is the only window that enables us to see directly the innermost part of an evolved massive stars, in which the angular momentum distribution and the equation of state are uncertain.

So far there has been extensive work devoted to studying gravitational radiation in rotational core collapse [2, 3, 4, 5, 6, 7, 8, 9] (see [10] for a review). More recently, Ott *et al.* [11] performed a large number of purely-hydrodynamic calculations employing a realistic equation of state (EOS) while neutrino transfer and microphysics are not treated. They investigated the effects of initial rotation rates and degree of differential rotation, on the gravitational waveforms (see also [4, 6]). On the other hand, Müller *et al.* [12] performed a small set of the rotational core collapse simulations while employing the elaborate neutrino transport with the detailed microphysics. Here it is noted that these recent [11, 12] studies took into account the initial models based on the recent stellar evolution calculations [13], which predict rather slow rotation rates at a presupernova stage than those assumed in the previous studies. If so, the peak amplitudes may not be obtained at core bounce but at the later phases when the neutrino-driven convections become active behind the accreting shock [12].

In addition to rotation, we study the effects of magnetic fields on the gravitational signals in this paper. In order to estimate the gravitational waveforms in the magnetohydrodynamic computations, we modify the conventional quadrupole formula including contributions from the electromagnetic fields. To our knowledge, the effects have not been investigated so far. To be rigorous, it is true that the realistic magnetorotational core collapse simulations should require the implementation of a realistic EOS, an adequate treatment of microphysics (weak interactions with neutrino transfer), and relativistic treatment of gravitation in three

dimensions. However it is far beyond our scope to treat them all at once. Thus, we choose to employ a realistic EOS and treat the microphysics in a simplified manner in the Newtonian gravity assuming axial symmetry. Recent stellar evolution studies show that the toroidal magnetic field components may be stronger than the poloidal ones prior to the collapse [13, 14]. We systematically change the strength of rotation and toroidal magnetic fields in a parametric way. By so doing, we hope to understand the effect of toroidal magnetic fields on the waveforms and the amplitudes of the gravitational wave both in the weak magnetic field ($\sim 10^{12}$ G) regime and in the strong magnetic field ($\sim 10^{15}$ G) regime at the formation of protoneutron star. The latter case may be associated with the formation of the so-called magnetars [15], such as anomalous X-ray pulsars and soft gamma-ray repeaters [16, 17]. Although the number of the magnetars is much smaller in comparison with the canonical pulsars, the gravitational wave from such objects should be investigated.

Furthermore, we investigate the effects of realistic EOS's on the gravitational signals. Needless to say, EOS is an important microphysical ingredient for determining the dynamics of core collapse, eventually, the gravitational wave amplitude. As a realistic EOS, Lattimer-Swesty EOS [18] has been used in recent simulations discussing gravitational radiation from rotational core collapse [11, 12]. It has been difficult to investigate the effects of the EOS's on the gravitational signals because available EOS's based on different nuclear models are limited (see, however, [19, 20, 21, 22]). Recently, a new complete EOS for supernova simulations has become available [23, 24, 25]. The EOS is based on the relativistic mean field (RMF) theory with a Thomas-Fermi approach. By implementing these realistic EOS's into the magnetohydrodynamic simulations, we first investigate the effects of the realistic EOS's on the gravitational wave signals.

We describe the numerical models in the next section. In the third section, we show the numerical results. A conclusion is given in the last section.

II. MODELS AND NUMERICAL METHODS

A. Initial Models

Recently, Heger *et al.* [13] performed the stellar evolution calculations , in which rotation and magnetic fields are taken into account. Remembering caveats that their calculations are

based on the one-dimensional models with uncertainties and not the final answer probably, they pointed out that the toroidal components of the magnetic fields are stronger than the poloidal ones at the presupernova stage. It is because the differential rotation amplifies the toroidal components by a convective stellar dynamo during the quasistatic stellar evolution [e.g., 14, 26]. To our knowledge, most of the past MHD simulations for investigating the dynamics of core collapse supernovae chosen the poloidal magnetic fields as the initial conditions. This situation motivates us to take the initial conditions, in which the toroidal components are dominant over the poloidal ones. Since Heger *et al.* [13] calculated only a small set of models so far, we prefer a parametric approach to construct the initial conditions in this paper.

We assume the following two rotation laws. In addition, we prepare the toroidal magnetic fields to yield the same profile as the rotation.

1. Shell-type rotation:

$$\Omega(r) = \Omega_0 \times \frac{{R_0}^2}{r^2 + R_0^2}, \tag{1}$$

$$B_\phi(r) = B_0 \times \frac{{R_0}^2}{r^2 + R_0^2}, \tag{2}$$

where $\Omega(r)$ is angular velocity, $B_\phi(r)$ is toroidal component of the magnetic fields, r is radius, and Ω_0, R_0 are model constants,

2. Cylindrical rotation:

$$\Omega(X, Z) = \Omega_0 \times \frac{{X_0}^2}{X^2 + {X_0}^2} \cdot \frac{Z_0^4}{Z^4 + Z_0^4}, \tag{3}$$

$$B_\phi(X, Z) = B_0 \times \frac{{X_0}^2}{X^2 + {X_0}^2} \cdot \frac{Z_0^4}{Z^4 + Z_0^4}, \tag{4}$$

where X and Z denote distances from the rotational axis and the equatorial plane, and X_0, Z_0 are model constants. The other parameters have the same meanings as above.

We have computed 14 models changing the combination of the total angular momentum, the rotation law, the degree of differential rotation, the total magnetic energy, and the equation of state. The model parameters are presented in Table I. The models are named after this combination, with the first letter, S (slow), M (moderate), R (rapid) representing the initial $T/|W|$, the second letter S (shell-type), C (cylindrical), denoting the rotation laws, the third letter, L (Long), S (Short), indicating the values of R_0, Z_0, which represent the degree of differential rotation, and the fourth letter, $7 \sim 0.3$, indicating the value of

$E_{\rm m}/|W|$. It is noted that the ratio of magnetic and rotational energies to gravitational energy are designated as $E_{\rm m}/|W|$ and $T/|W|$, respectively. We have chosen $\sim 10^{-3}, 0.5, 1.5\%$ for the initial $T/|W|$ and $\sim 10^{-7}, 10^{-4}, 10^{-2}, 10^{-1}, 10^{-0.3}(\sim 0.5)$ % for the initial $E_{\rm m}/|W|$. The initial poloidal components of magnetic fields are assumed to be uniform and parallel to the rotation axis, whose value is taken to be about four orders of magnitude lower than the toroidal components in accordance with the results by Heger *et al.* [13]. We employ the Lattimer-Swesty EOS in Model MSL4-LS, on the other hand, the relativistic EOS in the rest of the models. We have made precollapse models by taking a density, internal energy, electron fraction distributions from the spherically symmetric $15M_\odot$ model by Woosley and Weaver [27] and adding the angular momentum and the magnetic field according to the prescription stated above.

Heger *et al.* [13] pointed out that the iron core may rotate more slowly with the magnetic fields than without. It is because the magnetic braking reduces the angular momentum of the core during the quasistatic stellar evolution. Model SSL7 corresponds to the magnetorotational progenitor by them. We note that the models with the strongest magnetic fields are probably unrealistic as suggested from the results by Heger *et al.* [13]. However we prepared these models in order to cover the wide range of the field strength and to see the effects of the magnetic fields on the gravitational wave signals clearly.

B. Magnetohydrodynamics

The numerical method for MHD computations employed in this paper is based on the ZEUS-2D code [28]. The basic evolution equations are written as follows,

$$\frac{d\rho}{dt} + \rho\nabla\cdot\boldsymbol{v} = 0, \tag{5}$$

$$\rho\frac{d\boldsymbol{v}}{dt} = -\nabla P - \rho\nabla\Phi + \frac{1}{4\pi}(\nabla\times\boldsymbol{B})\times\boldsymbol{B}, \tag{6}$$

$$\rho\frac{d\left(\frac{e}{\rho}\right)}{dt} = -P\nabla\cdot\boldsymbol{v}, \tag{7}$$

$$\frac{\partial\boldsymbol{B}}{\partial t} = \nabla\times(\boldsymbol{v}\times\boldsymbol{B}) \tag{8}$$

$$\Delta\Phi = 4\pi G\rho, \tag{9}$$

TABLE I: The model parameters.

Model	$T/\|W\|(\%)$	$E_{\rm m}/\|W\|(\%)$	Rotation Law	R_0, X_0, Z_0 $\times 10^8$ (cm)	Ω_0 (s^{-1})	B_0 (G)
SSL7	3.2×10^{-3}	9.7×10^{-8}	Shell-type	$R_0 = 1$	0.1	5.0×10^9
MSL4	5.0×10^{-1}	10^{-4}	Shell-type	$R_0 = 1$	4.0	1.6×10^{11}
MSL2	5.0×10^{-1}	10^{-2}	Shell-type	$R_0 = 1$	4.0	1.6×10^{12}
MSL1	5.0×10^{-1}	10^{-1}	Shell-type	$R_0 = 1$	4.0	5.0×10^{12}
MSS4	5.0×10^{-1}	10^{-4}	Shell-type	$R_0 = 0.1$	63.4	3.5×10^{12}
MSS2	5.0×10^{-1}	10^{-2}	Shell-type	$R_0 = 0.1$	63.4	3.5×10^{13}
MSS1	5.0×10^{-1}	10^{-1}	Shell-type	$R_0 = 0.1$	63.4	1.1×10^{14}
MCS4	5.0×10^{-1}	10^{-4}	Cylindrical	$X_0 = 0.1, Z_0 = 1$	44.4	1.5×10^{12}
MCS2	5.0×10^{-1}	10^{-2}	Cylindrical	$X_0 = 0.1, Z_0 = 1$	44.4	1.5×10^{13}
MCS1	5.0×10^{-1}	10^{-1}	Cylindrical	$X_0 = 0.1, Z_0 = 1$	44.4	4.8×10^{13}
MCS0.3	5.0×10^{-1}	$10^{-0.3} \sim 0.5$	Cylindrical	$X_0 = 0.1, Z_0 = 1$	44.4	1.0×10^{14}
RCS1	1.5	10^{-1}	Cylindrical	$X_0 = 0.1, Z_0 = 1$	76.8	4.8×10^{13}
RCS0.3	1.5	$10^{-0.3} \sim 0.5$	Cylindrical	$X_0 = 0.1, Z_0 = 1$	76.8	1.0×10^{14}
MSL4-LS	5.0×10^{-1}	10^{-4}	Shell-type	$R_0 = 1$	4.0	1.6×10^{11}

where $\rho, \boldsymbol{v}, e, P, \boldsymbol{B}, \Phi$ are density, velocity, internal energy, pressure, magnetic field, gravitational potential, respectively. We denote the Lagrangian derivative as d/dt . The ZEUS-2D is an Eulerian code based on the finite-difference method and employs an artificial viscosity of von Neumann and Richtmyer to capture shocks. The time evolution of magnetic field is solved by the induction equation, Eq. (8). In so doing, the code utilizes the so-called constrained transport (CT) method, which ensures the divergence free ($\nabla \cdot \boldsymbol{B} = 0$) of the numerically evolved magnetic fields at all times. Furthermore, the method of characteristics (MOC) is implemented to propagate accurately all modes of MHD waves. The self-gravity is managed by solving the Poisson equation with the incomplete Cholesky decomposition conjugate gradient method. In all the computations, spherical coordinates are used and one quadrant of the meridian section is covered with 300 (r) $\times$ 50 (θ) mesh points. We made several major changes to the base code to include the microphysics. First, we added an equation for the electron fraction to treat electron captures and neutrino transport by

the so-called leakage scheme [29, 30, 31, 32]. The calculation of electron fraction is done separately from the main hydrodynamic step in an operator-splitting manner. Second, we implemented a relativistic EOS [23] or Lattimer-Swesty EOS [18] instead of the ideal gas EOS assumed in the original code. For a more detailed description of the methods, see Kotake *et al.* [33].

C. Gravitational wave signal from the magnetized stellar cores

Applying the methods [2, 3, 34], we derive the quadrupole formula in order to compute the gravitational waveforms from the magnetized stellar cores. The dimensionless gravitational wave amplitude $h_{\mu\nu} \equiv g_{\mu\nu} - \eta_{\mu\nu}$ can be calculated by the quadrupole formula as follows:

$$h_{ij}^{\rm TT}(R) = \frac{2G}{c^4}\frac{1}{R}\frac{d^2}{dt^2}I_{ij}^{TT}\left(t - \frac{R}{c}\right), \tag{10}$$

where i, j run from 1 to 3, t is the time, R is the distance from the source to the observer, the superscript "TT" means to take the transverse traceless part, and I_{ij} is the reduced quadrupole defined as

$$I_{ij} = \int \rho_*(x,t)\left(x_i x_j - \frac{1}{3}x^2\delta_{ij}\right) d^3x, \tag{11}$$

where ρ_* represents the total energy density including the contribution from the magnetic field,

$$\rho_* = \rho + \frac{B^2}{8\pi c^2}. \tag{12}$$

Expanding the right hand side of Eq. (10) in terms of the pure-spin tensor harmonics assuming axial symmetry shows that there is one nonvanishing quadrupole term, namely A_{20}^{E2}. Then one derives for the component of $h^{\rm TT}$ the following formula,

$$h_{\theta\theta}^{\rm TT} = \frac{1}{8}\left(\frac{15}{\pi}\right)^{1/2}\sin^2\alpha\ \frac{A_{20}^{\rm E2}}{R}, \tag{13}$$

where α is the angle between the symmetry axis and the line of the sight of the observer. Here $A_{20}^{\rm E2}$ is defined by the second time derivative of the mass quadrupole formula:

$$A_{20}^{\rm E2} = \frac{d^2}{dt^2}M_{20}^{\rm E2}, \tag{14}$$

where the mass quadrupole formula is given as

$$M_{20}^{\rm E2} = \frac{G}{c^4}\frac{32\pi^{3/2}}{\sqrt{15}}\int_0^1 d\mu \int_0^\infty dr\ \rho_*\left(\frac{3}{2}\mu^2 - \frac{1}{2}\right)r^4, \tag{15}$$

where $\mu = \cos\theta$. By a straightforward, however tedious, calculation to replace the time derivatives by the spatial derivatives applying the continuity equation, Eq. (5), the equation of motion, Eq. (6), and the induction equation, Eq. (8) noting the divergence-free constraint ($\nabla \cdot \boldsymbol{B} = 0$), $A_{20}^{\rm E2}$ can be transformed into the following form,

$$A_{20}^{\rm E2} \equiv A_{20\,,{\rm quad}}^{\rm E2} + A_{20\,,{\rm Mag}}^{\rm E2}, \tag{16}$$

where $A_{20\,,{\rm quad}}^{\rm E2}$ is the contribution from the matter:

$$\begin{aligned} A_{20\,,{\rm quad}}^{\rm E2} \;=\; & \frac{G}{c^4}\frac{32\pi^{3/2}}{\sqrt{15}}\Bigg(\int_0^1 d\mu \int_0^\infty r^2\, dr\, \rho[{v_r}^2(3\mu^2-1) + {v_\theta}^2(2-3\mu^2) - {v_\phi}^2 - 6 v_r v_\theta\, \mu\sqrt{1-\mu^2} \\ & -r\partial_r\Phi(3\mu^2-1) + 3\partial_\theta\Phi\, \mu\sqrt{1-\mu^2}] + \\ & \int_0^1 d\mu \int_0^\infty r^3\, dr[q_r(3\mu^2-1) - 3\; q_\theta\; \mu\sqrt{1-\mu^2}]\Bigg), \end{aligned} \tag{17}$$

$A_{20\,{\rm Mag}}^{\rm E2} \equiv A_{20\,j\times B}^{\rm E2} + A_{20\,\rho_{\rm m}}^{\rm E2}$ is the contribution from the magnetic field:

$$\begin{aligned} A_{20\,j\times B}^{\rm E2} \;=\; & \frac{G}{c^4}\frac{32\pi^{3/2}}{\sqrt{15}} \int_0^1 d\mu \int_0^\infty r^3\, dr\Big[(3\mu^2-1)\; \frac{1}{c}\; (\boldsymbol{j}\times\boldsymbol{B})_r - \\ & 3\mu\sqrt{1-\mu^2}\; \frac{1}{c}\; (\boldsymbol{j}\times\boldsymbol{B})_\theta\Big], \end{aligned} \tag{18}$$

$$\begin{aligned} A_{20\,\rho_{\rm m}}^{\rm E2} \;=\; & \frac{G}{c^4}\frac{32\pi^{3/2}}{\sqrt{15}} \int_0^1 d\mu \int_0^\infty dr\; \frac{1}{8\pi c}\frac{d}{dt}\Bigg[\frac{\partial}{\partial\theta}[B_r r^3(3\;\mu^2-1)]E_\phi - \frac{\partial}{\partial r}[B_\theta r^3(3\mu^2-1)]rE_\phi + \\ & +\; \frac{\partial}{\partial r}[B_\phi r^3(3\mu^2-1)]rE_\theta - \frac{1}{\sin\theta}\frac{\partial}{\partial\theta}[B_\phi \sin\theta r^3(3\mu^2-1)]E_r\Bigg]. \end{aligned} \tag{19}$$

$A_{20\,j\times B}^{\rm E2}, A_{20\,\rho_{\rm m}}^{\rm E2}$ represent the contribution from $j\times B$ part and from the time derivatives of the energy density of electro-magnetic fields, respectively. We take the first time derivative of the magnetic fields, because this is the leading order and the numerical treatments of the second time derivatives are formidable. Here, we write the gravitational amplitude as follows for later convenience,

$$h^{\rm TT} = h_{\rm quad}^{\rm TT} + h_{j\times B}^{\rm TT} + h_{\rho_{\rm m}}^{TT}, \tag{20}$$

where the quantities of the right hand of the equation are defined by Eqs. (13), (17), (18), and (19). It is noted that we take into account the terms related to the artificial viscosity (see Eq. (17), e.g., [2]). As mentioned, we employ an artificial viscosity of von Neumann and Richtmyer. The concrete form of q_i is,

$$q_i = \nabla_i\; [l^2\; \rho\; (\nabla\cdot\boldsymbol{v})^2], \tag{21}$$

where $i = r, \theta$ with l defining the dissipation length. In the following computations, we assume that observer is located in the equatorial plane since the gravitational wave radiates most in the plane ($\alpha = \pi/2$ in Eq. (13)), and that the source is assumed to be located at our galactic center ($R = 10$ kpc).

III. NUMERICAL RESULTS

A. Effects of the magnetic fields

We will first show the effect of the magnetic fields on the amplitude of the gravitational wave. For later convenience, the values of several important quantities are summarized in Tables II and III. We find that the amplitude is affected in the strongly magnetized models whose initial $E_{\rm m}/|W|$ is greater than 0.1 %. It is natural because the amplitude contributed from the magnetic fields should be an order of $R_{\rm mag}$ in comparison with the mass quadrupole moment component (see Eq. (12)), where

$$R_{\rm mag} = \frac{\frac{B_{\rm c}^2}{8\pi c^2}}{\rho_{\rm c}} \sim \ 10\ \% \left(\frac{B_{\rm c}}{\text{several } \times 10^{17}\ \text{G}}\right)^2 \left(\frac{\rho_{\rm c}}{10^{13}\ \text{g cm}^{-3}}\right)^{-1}, \tag{22}$$

with $B_{\rm c}, \rho_{\rm c}$ being the central magnetic field and the central density. Thus, strongly magnetized models, whose central magnetic fields at core bounce become as high as $\sim 10^{17}$ G, can affect the amplitude. As for the waveforms, we find that the contribution from $j \times B$ part dominates over one from the time derivatives of the energy density of electro-magnetic fields (see the left panel of Figure 1). Furthermore, it is found that the $j \times B$ part changes at the opposite phase of the matter quadrupole components (see the right panel of Figure 1). As a result, the negative parts of the amplitudes become less negative, while the positive parts become more positive. This lowers the peak amplitude at core bounce by an order of 10 % (see Table III). If the initial strength of the magnetic field is the same, the effect of the magnetic fields on the amplitude becomes more prominent for the fast rotation models (compare the values of ratio of MCS1 with RCS1, and MCS0.3 with RCS0.3 in Table III). This is because the central density at core bounce is lowered by the faster rotation (see Table II and Eq. (22)).

For the models, whose initial $E_{\rm m}/|W|$'s are less than 0.1%, the maximum amplitude is found to be determined by rotation as seen from Table II. We compare the waveforms for the

models MSL4 (left panel), MCS4 (right panel) in Figure 2. If we follow the commonly used categories of the waveforms [2, 4], the left panel shows type I behavior (relatively shorter intervals of the spikes) and the right panel type II behavior (longer intervals of the spikes). What determines the difference is the initial rotation rate and degree of differential rotation. It is found that type II occurs for the models with the strong differential rotation with a cylindrical rotation law as in the pure rotation case by Kotake *et al.* [35] and Ott *et al.* [11]. Furthermore, the sign of the values of the second peaks is found to be negative for the strongly differentially rotating models with a cylindrical rotation law, and positive for the other models (see Table IV). Note that by the "second peak" we mean where the absolute amplitude is second largest. Due to the $j \times B$ part, the second peaks with the positive values become more positive, while those with the negative values become generally less negative (see Table IV).

B. Effects of the equation of states

We compare the models MSL4 with MSL4-LS in this section. We repeat that these models differ from its employed EOS's. Other than this, any conditions, such as rotation, magnetic field, and the employed microphysics, are the same. Therefore the differences in the following purely reflect the influences of the employed EOS's. The most important difference of the two EOS's is the stiffness of the EOS's at nuclear matter density. In fact, the value of the incompressibility of the relativistic EOS (K = 281 MeV) is larger than that of Lattimer-Swesty EOS (K = 180 MeV). This means that the Lattimer-Swesty EOS is softer than the relativistic EOS. We note that there are three choices with different values of (K = 180, 220, 375 MeV) in the Lattimer-Swesty EOS. We take the most softest one in this calculation. This is because the value has been often employed for core collapse supernova studies.

A core bounce occurs when the central density reaches its peak of 3.2×10^{14} g cm^{-3}, 2.6×10^{14} g cm^{-3} at $t_{\rm b} = 215$ ms, 243 ms for the models MSL4-LS, MSL4, respectively. The earlier core bounce with the higher central density for the model MSL4-LS is due to the softness of the EOS. The softness of the Lattimer-Swesty EOS can be seen from Figure 3. The soft EOS results in the more smaller inner core of $M_{\rm ic} = 0.69 M_\odot$ than that of $M_{\rm ic} = 0.83 M_\odot$ by the relativistic EOS (see Table II). This result can be understood as

follows. The mass of inner core at core bounce is proportional to the square of the lepton fraction, Y_l. The electron capture with the neutrino emission proceeds further for the soft EOS because the core can contract more compact. As a result, the lepton fraction at core bounce becomes smaller, which results in the smaller mass of the inner core.

In the left panel of Figure 4, the gravitational waveforms for the models are presented. Shorter burst intervals for the model MSL4-LS are also due to the softness of the EOS. The duration of the burst are related to the typical dynamical timescale $\tau_{\rm dyn} \sim 1/\sqrt{G\rho_{\rm c}}$, where $\rho_{\rm c}$ is the central density. Since the values of $\rho_{\rm c}$ at the core bounce and the subsequent oscillations are larger for the soft EOS (see the right panel of Figure 4), the intervals of the burst become short. Although the collapse dynamics is changed by the differences of the EOS's, it is found that the values of the maximum amplitudes for the two models do not differ significantly (see Table II). This can be understood as follows. The amplitude of a gravitational wave is roughly proportional to the inverse square of the typical dynamical time scale, (see Eq. (10)). Since $t_{\rm dyn}$ is proportional to the inverse root of the central density, the amplitude becomes larger for the soft EOS by this factor. On the other hand, the amplitude is proportional to the value of the quadrupole moment, which becomes in turn small for the soft EOS due to the smaller inner core. The maximum amplitude is determined by the competition between these factors. As a result, the amplitude becomes almost the same for the Lattimer-Swesty EOS and the relativistic EOS.

In our calculations, we note that there are no models that correspond to the so-called type III waveform, which occurs only when a EOS is very soft before core bounce [4]. This is because the relativistic EOS and Lattimer-Swesty EOS is not so soft in the corresponding regime.

C. The gravitational wave properties in the weakly magnetized and slowly rotating model

We show the properties of the waveform with collapse dynamics in the model SSL7. It is noted that the initial condition for the model is based on the recent stellar evolution calculation [13]. We repeat that the initial $T/|W|$ and $E_{\rm m}/|W|$ are much smaller than the other models. The model bounces at $t = 215$ msec at a central density of 3.0×10^{14}g cm^{-3}. It occurs not by rotation or magnetic fields but by the stiffening of the equation of state. After

the core bounce, very weak signals are lasting (see Fig. 5). The gravitational amplitudes from the bounce and later reexpansion phases are three orders of magnitude smaller than the other models. The timescale of the spikes ($\sim$ msec) is determined by the small scale non-radial motions behind the shock wave.

D. Maximum amplitude and second peak

In Figure 6, the absolute values of the maximum amplitudes and second peaks are presented. Note that the data points are confined to small regions although we explore the wide range of the initial magnetic field strength. This is because the magnetic fields lower the peak ampitudes by $\sim 10\%$ but do not change the typical frequencies of the gravitational waves significantly. Thus the maximum amplitudes and the typical frequencies are mainly determined by rotation. The maximum amplitudes are mainly clustered in the two regions (see the open squares in Figure 6). One is around $\sim$ 100 Hz for the models whose names begin with "R" (rapidly rotating models) and another is around from $\sim$ 300 Hz to $\sim$ 500 Hz for the models whose names begin with "M" (moderately rotating models). The values of the maximum amplitudes are in the range of $3.5 \times 10^{-23} \leq h^{\rm TT} \leq 2.6 \times 10^{-20}$. The smallest value is from model SSL7, whose initial model is taken from the recent stellar evolution calculation. If the model is correct, it should be difficult to detect the gravitational wave even for the next generation detectors such as advanced LIGO and LCGT unless a supernova occurs very close to us (see Figure 6). When we compare the maximum amplitudes from model MSL4 (relativistic EOS) with that from model MSL4-LS (Lattimer-Swesty EOS), no significant differences are found, except that the typical frequency for LS EOS becomes slightly higher due to the softness of the EOS (see Figure 6). Therefore the features of the gravitational wave are almost independent of the realistic EOS's.

As pointed out earlier, we found that the signs of the values of the second peaks are negative for models with strongly differential rotation with a cylindrical rotation law and positive for the others (see Table III). The absolute amplitudes of the second peak are also presented in Figure 6. As shown, they are within the detection limit of first LIGO for a source at a distance of 10 kpc, although the absolute values of the negative values are reduced by the magnetic fields. In addition, it is quite likely that the detectors in the next generation, such as advanced LIGO and LCGT, to detect the difference. We will obtain

information about the angular momentum distribution of evolved massive stars, if we can detect the differences by observations of the gravitational wave. However, it seems difficult to get information about the distributions of the magnetic fields only by the gravitational wave from the magnetorotational core collapse. We note that the effects of the magnetic fields on the signals may become important after the formation of the strongly magnetized star. As pointed [40, 41], the gravitational waves, which are detectable for interferometers such as LIGO, may be emitted by the global rearrangement of the strongly magnetic fields ($B > 10^{16}G$) in the core.

IV. CONCLUSION

We have done a series of two-dimensional magnetohydrodynamic simulations of the rotational collapse of a supernova core and calculated gravitational waveforms. We have modified the conventional quadrupole formula in order to include the contributions from the electromagnetic fields. Recent stellar evolution calculations imply that the magnetic field of the toroidal component is much stronger than that of the poloidal ones at the presupernova stage. In this study, we systematically investigate the effects of the toroidal magnetic fields on the gravitational waveforms. We have employed the two kinds of the realistic equation of states, which are often used in the supernova simulations. By so doing, we have investigated the effects of the equation of sates on the gravitational signals. As for the microphysics, we took into account electron capture and neutrino transport in an approximate method. We found the following.

(1). Effects of the magnetic field on the amplitude and the waveform of the gravitational waves appear for the strongly magnetized models, whose initial $E_{\rm m}/|W|$'s are greater than 0.1%. As for the contributions from the magnetic field, the $j \times B$ part is found to dominate over the time derivatives of the magnetic energy. Since $j \times B$ part changes with the opposite phase in comparison with the mass quadrupole moment components, the maximum amplitudes are lowered by an order of 10% for the strongly magnetized models. However, the maximum amplitudes are mostly within the detection limits of the detectors of TAMA and first LIGO if a source is located at a distance of 10 kpc.

(2) The maximum amplitudes do not change significantly if we employ the two realistic

TABLE II: Summary of important quantities for all models. $t_{\rm b}$ is the time of bounce, $\rho_{\rm maxb}$ is the maximum density at bounce, $M_{\rm i.c\,b}$ is the mass of inner core at bounce, $T/|W|_{\rm final}, E_{\rm m}/|W|_{\rm final}$ is the final ratio of rotational and magnetic energies to gravitational energy of the core, respectively. Δt is the duration time full width at half maximum of the first burst, and $|h^{\rm TT}|_{\rm max}$ is the maximum amplitude, including the contributions from the electromagnetic fields. Note that we speak of the inner core, where the matter falls subsonically, which corresponds to the unshocked region after core bounce.

Model	$t_{\rm b}$	$\rho_{\rm maxb}$	$M_{\rm i.c\,b}$	$T/\|W\|_{\rm final}$	$E_{\rm m}/\|W\|_{\rm final}$	Δt	$\|h^{\rm TT}\|_{\rm max}$
	(ms)	(10^{14} g cm^{-3})	($M_\odot$)	(%)	(%)	(ms)	(10^{-20})
SSL7	214.6	2.97	0.61	1.0×10^{-2}	3.5×10^{-8}	0.75	3.5×10^{-3}
MSL4	242.8	2.61	0.83	8.7	4.3×10^{-5}	0.74	1.66
MSL2	242.9	2.66	0.83	8.6	4.2×10^{-3}	0.73	1.66
MSL1	242.7	2.65	0.83	8.6	3.9×10^{-2}	0.73	1.65
MSS4	241.8	1.72	0.87	9.0	2.9×10^{-4}	0.58	1.78
MSS2	242.0	1.71	0.87	9.0	2.9×10^{-2}	0.58	1.80
MSS1	242.1	2.10	0.87	9.1	2.4×10^{-1}	0.58	1.87
MCS4	245.1	1.45	0.91	9.9	3.0×10^{-4}	0.53	2.54
MCS2	244.1	1.55	0.91	10.0	2.7×10^{-2}	0.53	2.58
MCS1	244.2	1.88	0.91	10.1	1.8×10^{-1}	0.53	2.63
MCS0.3	245.3	2.25	0.91	10.0	5.8×10^{-1}	0.53	2.34
RCS1	302.2	0.17	1.11	12.2	3.1×10^{-1}	2.03	0.90
RCS0.3	320.5	0.84	1.14	12.2	8.0×10^{-1}	1.76	1.14
MSL4-LS	215.4	3.20	0.69	8.2	3.4×10^{-5}	0.63	1.62

equation of states commonly used in the supernova simulations. Since Lattimer-Swesty EOS is softer than the relativistic EOS, the mass of the inner core for the Lattimer-Swesty EOS becomes small, which reduces the mass quadrupole moments at core bounce. On the other hand, the softness allows the core to contract deeply, which makes the central density larger at core bounce. By the competition of these factors, the maximum amplitude remains

TABLE III: Effects of the strong magnetic fields on the maximum amplitudes. Note that all the values of the amplitudes of the gravitational wave are given in unit of 10^{-20} in this table.

Model	$h^{\rm TT}_{\rm quad}$	$h^{\rm TT}_{j\times B}$	$h^{\rm TT}_{\rho_{\rm m}}$	$\lvert h^{\rm TT}_{j\times B}/h^{\rm TT}_{\rm quad}\rvert(\%)$
MSL1	- 1.65	2.40×10^{-2}	-8.56×10^{-4}	1.5
MSS1	- 2.16	2.95×10^{-1}	-1.04×10^{-3}	13.8
MCS1	- 2.69	6.46×10^{-2}	-1.01×10^{-3}	2.4
MCS0.3	- 2.55	2.13×10^{-1}	-4.63×10^{-3}	8.3
RCS1	- 1.01	1.11×10^{-1}	-2.45×10^{-3}	10.9
RCS0.3	- 1.53	3.83×10^{-1}	-1.92×10^{-3}	25.0

almost the same between the two realistic EOS's. We note the difference that the typical frequencies of the gravitational waves for the Lattimer-Swesty EOS become higher due to the softness of the EOS. These effects of the EOS's on the gravitational waves are found to be independent of those of the magnetic fields, since the strong magnetic fields change the maximum amplitudes and do not change the typical frequencies of the gravitational waves.

(3) For the weakly magnetized models, whose initial $E_{\rm m}/|W|$'s are smaller than 0.1%, the gravitational wave amplitude and the waveform are determined by rotation as in the pure rotation case [35]. The waveforms are categorized into the conventional criteria [4]. The maximum amplitudes are within the detection limits for the detectors of TAMA and first LIGO for a supernova at a distance of 10 kpc. From the model based on the recent stellar evolution calculation, it seems difficult to detect the gravitational wave unless a supernova occurs very close to us. Type III does not occur if the two realistic EOS's are employed.

(4) The signs of the values of the second peaks are found to be negative for the strongly differentially rotating models with a cylindrical rotation law, and positive for the other models. Due to the $j \times B$ part of the electromagnetic contributions, the positive values of the second peak become more positive, while the negative values become less negative. However the absolute values of the second peaks are within the detection limit of the first LIGO for a supernova at a distance of 10 kpc. It means that it will give us information about the angular momentum distribution of massive evolved star if a supernova occurs at our galactic center. On the other hand, it seems difficult to extract the information about

TABLE IV: Some characteristic quantities for the waveform analysis. The names of the models whose initial rotation law is cylindrical with strong differential rotation are written in bold letters. $T^I_{\rm osc}$ and $T^{II}_{\rm osc}$ the first and second oscillation period of the inner core, respectively. $h^{TT}_{\rm second}$ is the amplitude of gravitational wave at the second peak.

Model	$T^I_{\rm osc}$ [ms]	$T^{II}_{\rm osc}$ [ms]	$h^{TT}_{\rm second}$ [10^{-20}]
MSL4	1.9	1.3	0.93
MSL2	1.9	1.1	0.93
MSL1	2.0	1.2	1.02
MSS4	2.4	2.8	0.87
MSS2	2.5	2.7	0.88
MSS1	2.5	2.8	1.03
MCS4	3.1	2.7	- 0.62
MCS2	3.1	2.7	- 0.61
MCS1	3.1	2.7	- 0.63
MCS0.3	3.2	2.7	- 0.57
RCS1	11.2	9.1	- 0.47
RCS0.3	11.4	9.2	- 0.53
MSL4-LS	1.5	1.1	1.00

the magnetic field only by the gravitational wave from a magnetorotational collapse of a supernova. By the lack of the significant features by the magnetic fields in the gravitational signals in addition to those by rotation, a weak upper limit of the initial magnetic field strength of $\sim 10^{14}$ G in the central core prior to gravitational collapse may be put.

Finally, we state some discussions based on the results in this study. In all the models, the final rotation rates are within the critical value where Maclourion spheroids become secularly unstable against triaxial perturbations ($T/|W|_{\rm final} < 13.75\%$). Therefore, the axial symmetry assumed in this study may be justified. It is also noted that Rampp et al. [5], who performed the three-dimensional (3D) rotational core-collapse simulations, suggest that the features of the gravitational signals do not differ significantly from those by the two-

dimensional simulations. However, it is necessary to perform the 3D simulations for the more realistic estimation of the gravitational wave signals. As for the magnetic field contributions, the entanglement of the field lines in the azimuthal direction may suppress the gravitational radiation for a given rotation rate. Furthermore, it is noted that the non-axisymmetric motions of the matter produce the cross modes of the gravitational waves, which vanish in case of axial symmetry [43, 44]. From the recent results by Fryer & Warren (2003) [44], who did 3D rotational core-collapse simulations, the maximum amplitude of the cross modes was presented to be $\sim 10^{-22}$ at several 100 Hz for a supernova in our galactic center. Although this value is smaller than that of the plus modes, the value seems to be within the detection limits of the gravitational wave detectors in the next generation, such as advanced LIGO and LCGT. If the characteristics of the waveforms between the plus and cross modes are detected, we think that it may be a good tool to extract information not only about rotation but also about magnetic fields in the evolved massive star. In order to investigate this, we are currently preparing for the 3D MHD simulations (H. Sawai et al. 2004 in preparation).

Recent observations imply that gamma-ray bursts (GRBs) are associated with core-collapse supernovae [45, 46]. Although the failed supernova or the so-called collapsar model are supposed to be probable [47, 48], it is still controversial what powers GRBs. As the energy source for fireballs, the energy deposition by neutrinos emitted from the accretion disk or by the MHD process which extracts the angular momentum of the rotating black hole are considered to be important. MacFadyen *et al.* [49] reported that matter with the mass of $\sim 0.1-5M_{\odot}$ falls into the central black hole during minutes to hours, which suggests the duration for the activity of GRBs. It is noted that no magnetic fields are considered in their calculations. When we boldly extrapolate the central magnetic fields in our strongest magnetized models, which become as high as $\sim 10^{17}$ G in the central region, to the model of GRBs, it may not seem so unnatural to imagine the infall of the strongly magnetized material into the black hole. If the magnetized matter falls into the black hole anisotropically, we expect the emission of the gravitational waves. In order to calculate the amplitudes, the formula, which we derived in this paper, will be useful. Here it should be noted that the fully general relativistic magnetohydrodynamic simulations with the multi-dimensional neutrino transport are required for the reliable estimation to determine the masses of the black hole and the accretion disk. Therefore further advancements in the numerical simulations are necessary for the quantitative discussions.

Recently, one group claims the detection of linear polarization of $\sim$ 80 % in a GRB [50], however, the other group claims that the polarization is less than $\sim$ 4 % [51]. The discrepancy may come from the difference in the way of data analysis. If the former is correct, it may seem consistent with our results, which predict rather coherent magnetic fields in the vicinity of the central core.

As stated earlier, Müller *et al.* [12] recently reported that the maximum amplitude is not obtained at the core bounce but at the later phases when the anisotropic neutrino radiation becomes active (see, also, [42, 43]). If the degree of the anisotropy of neutrino radiation could be observed from the gravitational radiation, it will help to understand the explosion mechanism itself. This is because anisotropic neutrino radiation induced by rotation is likely to produce an asymmetric explosion [33, 44, 52] as suggested by observation of SN 1987 A [53, 54, 55, 56]. Unfortunately, this is beyond our scope now to estimate the effects of anisotropic neutrino radiation on the gravitational signals by our crude treatment of the neutrino transport. For the purpose, we are now developing a two-dimensional neutrino transport code, which is indispensable for the estimation of the gravitational wave from the anisotropic neutrino radiation.

Acknowledgments

We are grateful to K. Numata and M. Ando for helpful discussions. K.K would like to be thankful to M. Shimizu and M. Oguri for supporting computer environments. The numerical calculations were partially done on the supercomputers in RIKEN and KEK (KEK supercomputer Projects No.02-87 and No.03-92). This work was partially supported by Grants-in-Aid for the Scientific Research from the Ministry of Education, Science and Culture of Japan through No.S 14102004, No. 14079202, and No. 14740166.

---

[1] C. Cutler and K. S. Thorne, to appear in Proceedings of GR16 (Durban, South Africa, 2001).

[2] R. Mönchmeyer, G. Schäfer, E. Müller, and R.E. Kates, Astron. Astrophys. **246**, 417, (1991).

[3] S. Yamada and K. Sato, Astrophys. J. **450**, 245, (1995).

[4] T. Zweger and E. Müller, Astron. Astrophys. **320**, 209, (1997).

[5] M. Rampp, E. Müller, and M. Ruffert, Astron. Astrophys. **332**, 969R, (1998).

[6] H. Dimmelmeier, J.A. Font, and E. Müller, Astron. Astrophys. **393**, 523D, (2002).

[7] C.L. Fryer, D.E. Holz, and S.A. Hughes, Astrophys. J. **565**, 430, (2002)

[8] M. Shibata, Phys. Rev. D. **67**, 024033 (2003).

[9] M. Shibata and Y. Sekiguchi, Phys. Rev. D , **68**, 104020, (2003).

[10] K.S. New, accepted for publication in Living Reviews in Relativity, gr-qc/0206041.

[11] C.D. Ott, A. Burrows, E. Livne, and R. Walder, Astrophys. J. 2003. (to be published).

[12] E. Müller, M. Rampp, R. Buras, H.-T. Janka, and D.H. Shoemaker 2003, submitted to Astrophys. J.

[13] A. Heger, S.E. Woosley, N. Langer and H.C. Spruit, to appear in Proc. IAU 215 "Stellar Rotation" (2003).

[14] H.C. Spruit, Astron. Astrophys. **381**, 923, (2002).

[15] R.C. Duncan and C. Thompson, Astrophys. J. Lett. **392**, L9, (1992).

[16] O.H. Guseinov, E. Yazgan, A. Ankay, and S.O. Tagieva, 1, **1**, Int. J. Mod. Phys. D. (2003).

[17] B. Zhang and A. Kharding, Astrophys. J. Lett. **535**. L51, (2000).

[18] J.M. Lattimer and F.D. Swesty, Nucl. Phys. A. **535**, 331, (1991).

[19] S.W. Bruenn, Astrophys. J. Suppl. **62**, 331 (1986).

[20] S.W. Bruenn, Astrophys. J. **340**, 955, (1989).

[21] S.W. Bruenn, Astrophys. J. **341**, 385, (1989).

[22] F.D. Swesty, J.M. Lattimer and E.S. Myra, Astrophys. J. **425**, 195, (1994).

[23] H. Shen, H. Toki, K. Oyamatsu, and K. Sumiyoshi, Nucl. Phys. **A637**, 43, (1998).

[24] H. Shen, H. Toki, K. Oyamatsu, and K. Sumiyoshi, Prog. Theor. Phys. **100**,1013, (1998).

[25] K. Sumiyoshi, H. Suzuki, S. Yamada, and H. Toki, Nucl. Phys. A in press.

[26] E.N. Parker, Cosmological magnetic fields: The origin and their activity, Oxford, Clarendon Press, (1979).

[27] S.E. Woosley, and T.A, Weaver, private communication, (1995).

[28] J.M. Stone, and M.L. Norman, Astrophys. J. Supl. **80**, 791, (1992).

[29] R.I. Epstein, and C.J. Pethick, Astrophys. J. **243**, 1003, (1981).

[30] S.A. Bludman, I. Lichtenstadt, and G. Hayden, Astrophys. J. **261**, 661, (1982).

[31] K.A. van Riper, and J.M. Lattimer, Astrophys. J. **249**, 270, (1981).

[32] K.A. van Riper, Astrophys. J. **257**, 793, (1982).

[33] K. Kotake, S. Yamada, and K. Sato, Astrophys. J. **595**, 304, (2003).

[34] S. Yamada and H. Sawai, submitted to Astrophys. J. (2003).

[35] K. Kotake, S. Yamada, and K. Sato, Phys. Rev. D. **68**, 44023, (2003).

[36] M. Ando and TAMA collaboration, Class. Quantum Grav. **19**, 1409, (2002).

[37] K.S. Thorne, Gravitational Waves. In *Proceedings of the Snowmass 95 Summer Study on Particle and Nuclear Astrophysics and Cosmology,* World Scientific, pp. 398-425, (1995).

[38] A. Weinstein, Class. Quantum Grav. **19**, 1575, (2002).

[39] LCGT Collaboration, Int. J. Mod. Phys. D, **5**, 557, (1999).

[40] K. Ioka, Mon. Not. R. Soc. **327**, 639, (2001).

[41] R. Lapiedra and J. A. Miralles, Astron. Astrophys. **403**, 419, (2003).

[42] A. Burrows, and J. Hayes, Phys. Rev. Lett. **76**, 352, (1996).

[43] E. Müller, and H.-T. Janka, Astron. Astrophys. **317**, 140, (1997).

[44] C.L. Fryer, M.S. Warren, 2003, Astrophys. J. (to be published).

[45] T. Galama, et al, Nature, **395, 670, (1998)**.

[46] K. Z. Stanek, et al, Astrophys. J. **591** ,L17, (2003).

[47] S. E. Woosley, Astrophys. J, **405**, 273, (1993).

[48] A. I. MacFadyen and S. E. Woosley, Astrophys. J, **524**, 262, (1999).

[49] A. I. MacFadyen, S. E. Woosley, and A. Heger, Astrophys. J, **550**, 410, (2001).

[50] W. Coburn and Boggs. S. E, Nature. **423**, 415, (2003).

[51] R. E. Rutledge and D. B. Fox, submitted to Mon. Not. R. Soc. (2003).

[52] T.M. Shimizu, T. Ebisuzaki, K. Sato, and S. Yamada, Astrophys. J. **552**, 756, (2001).

[53] L. Wang, J.C. Wheeler, Z. Li, and A. Clocchiatti, Astrophys. J. **467**, 435, (1996).

[54] C.S.J. Pun and The Supernova Intensive Studies (SNIS). Collaboration. 2001, AAS Meeting, 199, 94. 02.

[55] L. Wang, D.A. Howell, P. Höflich, and J.C. Wheeler, Astrophys. J, **550**, 1030, (2001).

[56] L. Wang et al. Astrophys. J. **579**, 671, (2002).

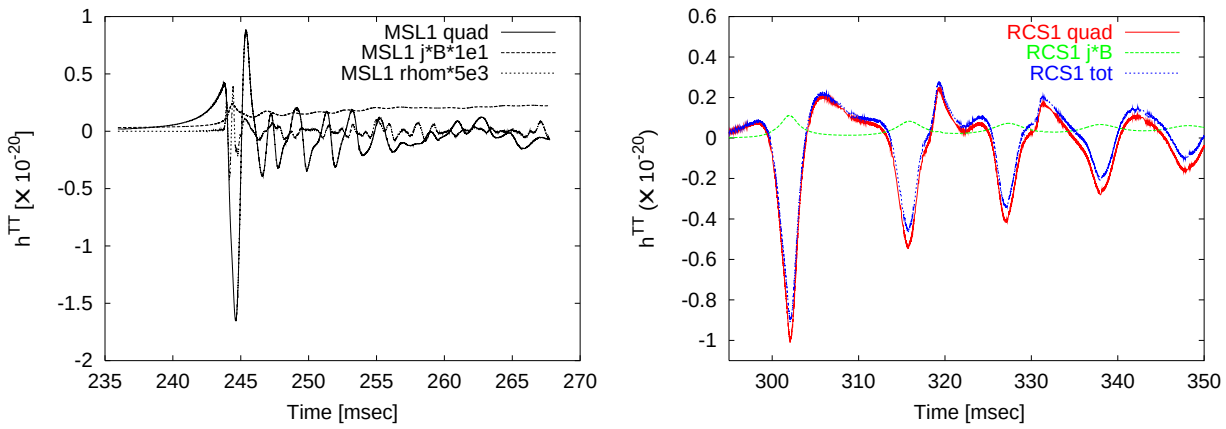

FIG. 1: Waveforms for models MSL1 (left panel), RCS1 (right panel). In the left panel, "quad", "$j\times B$", and "rhom" ($\rho_{\rm m}$) represents the contribution from the mass quadrupole moment, $j\times B$ part, and the time derivatives of the magnetic energy density ($\rho_{\rm m}$ part), respectively. The amplitudes are artificially multiplied by 10^1 for $j \times B$ part and 5×10^3 for $\rho_{\rm m}$ part to make their waveforms clear. From the panel, $j \times B$ part is found to dominate over $\rho_{\rm m}$ part. In the right panel, "tot" indicates the amplitude including the total contributions. From the panel, it is found that the $j \times B$ part changes at the opposite phase of the mass quadrupole moment. Note that the source is assumed to be located at the distance of 10 kpc.

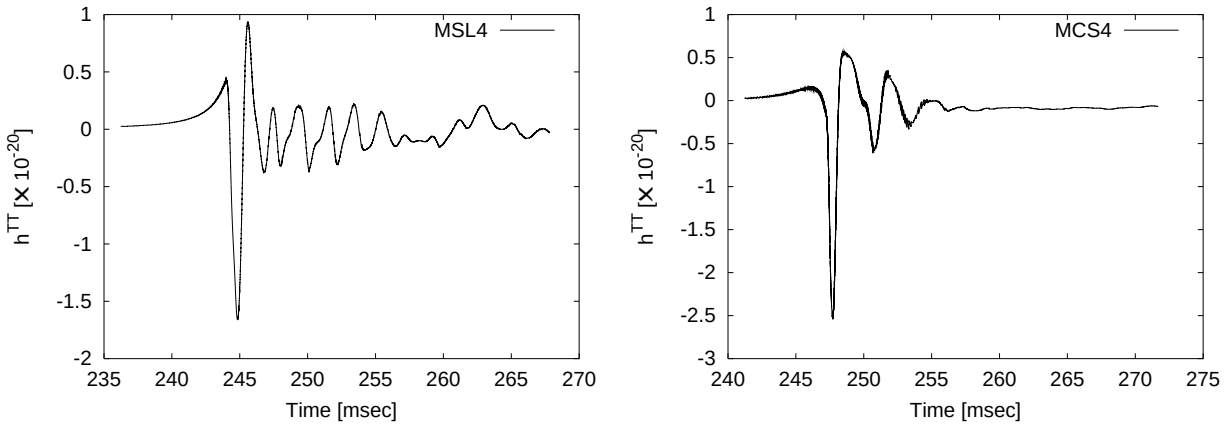

FIG. 2: Waveforms for models MSL4 (left panel), MCS4 (right panel). Note that the source is assumed to be located at the distance of 10 kpc.

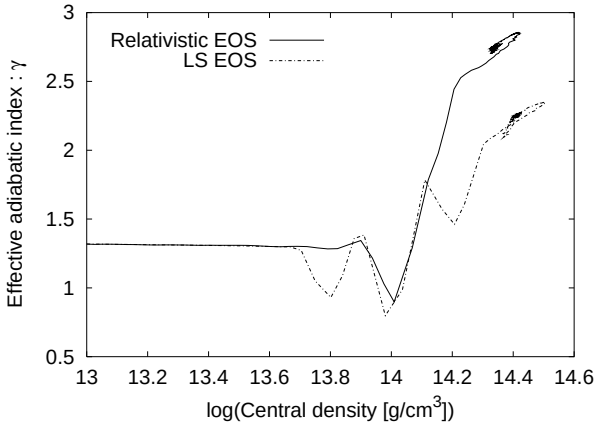

FIG. 3: Relation between the central density and the effective adiabatic index γ at near core bounce. Relativistic EOS, LS EOS in the figure represents the relation taken from the values from the models MSL4 and MSL4-LS, respectively. The swirls at the density of $\sim 10^{14.4}$ g cm^{-3} are due to the reexpansion of the core after core bounce.

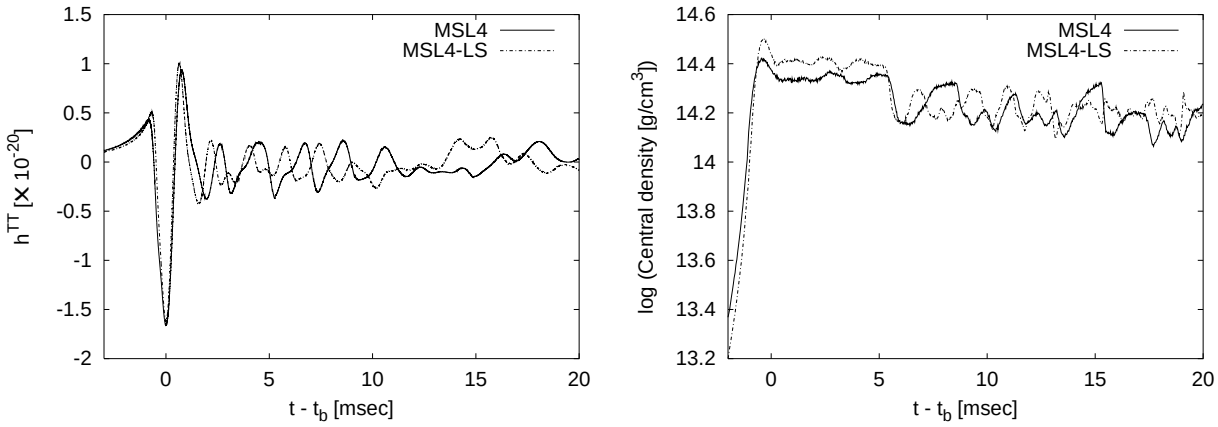

FIG. 4: Waveforms (left panel) and the time evolution of the central density (right panel) for models MSL4 (left panel), MSL4-LS (right panel). All times are relative to the time of bounce ($t_{\rm b}$) in this figure. Note that the source is assumed to be located at the distance of 10 kpc.

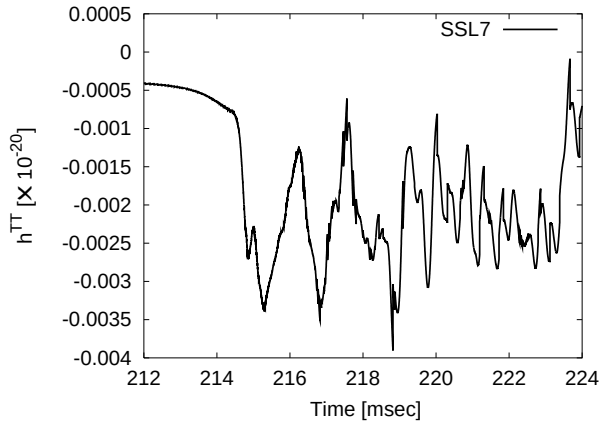

FIG. 5: Waveform for model SSL7, which is based on the recent stellar evolution calculation. The amplitudes are about three orders of magnitudes smaller than the other models. Note that the source is assumed to be located at the distance of 10 kpc.

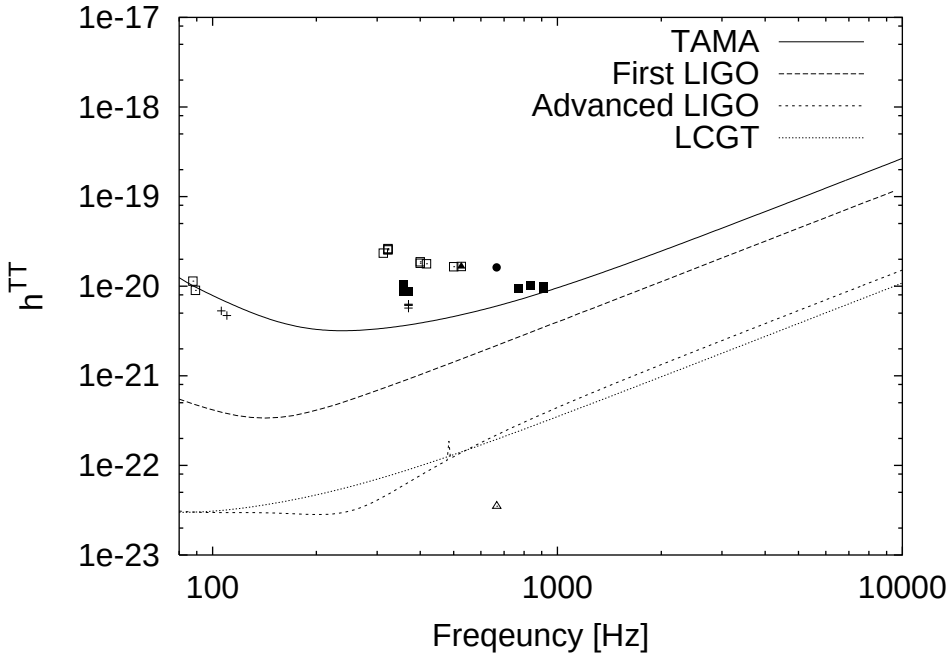

FIG. 6: Detection limits of TAMA [36], first LIGO [37], advanced LIGO [38], and Large-scale Cryogenic Gravitational wave Telescope (LCGT) [39] with the expected amplitudes from numerical simulations. The open squares represent the maximum amplitudes for all the models, except for models MSL4 (closed triangle) and MSL4-LS (closed circle). On the other hand, the pluses and the closed squares represent the amplitudes of second peaks for models with strong differential rotation with a cylindrical rotation law and for the other models, respectively. Open triangle represents the maximum amplitude for model SSL7. We estimate the characteristic frequencies by the inverse of duration periods of the corresponding peaks. Note that the source is assumed to be located at the distance of 10 kpc.